Acta Mech 228, 2759–2773 (2017)
DOI 10.1007/s00707-015-1525-x

ORIGINAL PAPER

Hideo Koguchi · Koki Yokoyama

Stress analysis in three-dimensional joints with a crack at the vertex of the interface

In case of mode II

Received: 16 May 2015 / Revised: 5 August 2015 / Published online: 21 December 2015

Abstract A crack initiates frequently at a vertex in three-dimensional joints under an external load and a thermal load. In the present paper, the stress distributions near a very small crack occurring at the vertex of the interface in a three-dimensional joint are analyzed under a tensile load using a boundary element method, and the stress intensity factor of mode II is investigated along the crack front. The joint model is composed of silicon and resin, which is modeled on a material combination in electronic devices. Three kinds of crack shape, triangular, quarter circular, and concave shapes, are supposed as a crack shape. First, the stress distributions near the vertex in the model without a crack are obtained and are used for normalizing the singular stress at the front of the crack. Dimensionless stress intensity factor for an interface crack is defined and determined from the distribution of the normalized stress. Next, the stress distribution near the intersection point of the crack front and the side surface is precisely investigated. An eigenanalysis at the intersection point is conducted, and eigenvalues yielding the stress singularity are obtained. Then, it is found that there are two values yielding the stress singularity. The stress distributions near the intersection point are expressed using the angular functions for each value yielding the singularity. Finally, it is shown that the stress intensity factor for mode II along the crack front varies following the summation of functions composed of the distance from the intersection point with the power indices of $(0.5 - \lambda_1)$ and $(0.5 - \lambda_2)$, where λ_1 and λ_2 are the orders of stress singularity at the intersection point.

1 Introduction

It is well known that singular stress fields occur at the edge of the interface in dissimilar material joints due to the mismatch of material properties. When an external force or a temperature change is applied to the joints, cracks initiate near the interface due to the singular stress fields. Then, the failure of joints frequently occurs.

In case of one real singularity, the singular stress fields in two-dimensional joints can be expressed in a polar coordinate system, where an origin is located at the edge, as

$$\sigma_{ij}(r, \vartheta) = \widehat{K}_1 g_{1ij}(\vartheta) r^{-\lambda} + \widehat{K}_2 g_{2ij}(\vartheta) \tag{1}$$

where r is a distance from the edge of the interface, ϑ is an angle from an axis along the interface, λ is the order of the stress singularity, $\widehat{K}_1$ is the intensity of the singularity, and $g_{mij}(\vartheta)$ $(m = 1, 2)$ is an angular function.

Bogy [1,2] derived an eigenequation for determining the order of stress singularity using Dundurs' parameters [3]. After that, a lot of research on singular stress fields in two-dimensional joints has been done

H. Koguchi (✉) · K. Yokoyama
1603-1 Kamitomioka, Nagaoka, Niigata 940-2188, Japan
E-mail: koguchi@mech.nagaokaut.ac.jp
Tel.: +81-258-47-9734
Fax: +81-258-47-9770

until now, and several methods for analysis were developed, such as a conservative integral, a finite element method using an enriched element, and a singular element [4–13]. Recently, Hwu et al. [15] proposed a new unified expression for the analytical solutions of singular stresses at almost all possible interface corners. They presented a method for analyzing a newly defined stress intensity factor using the path-independent H-integral. The definition includes the ordinary stress intensity factors of the crack. On the contrary, there are not so much studies on three-dimensional stress singularity in three-dimensional joints [16–27]. Mittelstedt and Becker [19] developed a numerical method referred to as the boundary finite element method and used for the investigation of the orders and modes of three-dimensional stress singularities which occur at notches and cracks in isotropic half-spaces as well as at free edges and free corners of layered plates. Koguchi et al. [28,29] have studied the order of stress singularity and singular stress fields in three-dimensional joints, and demonstrated that the singular stress lines also largely influence the characteristics of singular stress fields near the vertex of the interface. On the other hand, studies on the stress intensity factors in three-dimensional cracks have been continuously conducted [14,30–33]. Nagai et al. [30] proposed a method for determining the stress intensity factors in a three-dimensional interface crack between dissimilar anisotropic materials using the H-integral. Zhu et al. [31] developed an extended hypersingular integro-differential equation method for modeling the 3D interface crack problem in fully coupled electromagnetothermoelastic anisotropic multiphase composites under extended electromagnetothermoelastic-coupled loads by theoretical analysis and numerical simulations. Recently, Veluri and Jensen [33] analyzed the steady-state propagation of interface cracks in thin surface layers close to three-dimensional corners. Kuo and Hwu [14] proposed a definition of the multi-order stress intensity factors and showed the distributions of the stress intensity factors along the crack tip in three-dimensional joint models using a domain-independent H-integral. In the previous analyses for surface cracks, the values of the stress intensity factor were obtained at any discrete points along the crack front and were investigated from a point on the crack tip to a point on the side free surface. The distributions against the distance from the free surface frequently vary near the surface; furthermore, it is unclear whether the stress intensity factor varies following any law or not. In this case, some numerical errors may exist in the values near the free surface since the singular stress fields with a different index from -0.5 exist at the intersection point with the free surface and the crack front. In our study, the stress intensity factor for the interface crack is evaluated from the singular stress fields around the intersection point, i.e., the direction in the analysis is the one from a point on the side surface to a point on the crack tip. It is supposed that an accurate value for the stress intensity factor near the free surface can be evaluated by the analysis of singular stress near the intersection point of the free surface and crack front.

From the previous studies, singular stress fields at the vertex of the interface in three-dimensional joints can be described as $\sigma_{ij}\,(r,\theta,\phi) = K_1 f_{1ij}\,(\theta,\phi)\, r^{-\lambda} + K_2 f_{2ij}\,(\theta,\phi)$ in a spherical coordinate system, where r is the distance from the origin of the singular stress field, θ and ϕ are angular variables, K_1 is the intensity of the singularity, and f_{1ij} are angular functions for stresses σ_{ij}. In the case of $0 < \lambda < 1$, it can be said that the stress field has a singularity. The angular functions have singularities with respect to the angle ϕ of a singular stress line, λ_{line}, and interface crack tip, $-0.5 \pm i\varepsilon$. The stress intensity factors corresponding to complex angular functions for $-0.5 \pm i\varepsilon$ are defined, and the angular functions are normalized by the values at the interface of the angular function. Then, the stress intensity factors of the interface crack are defined using the angular function in a three-dimensional interface crack. In particular, the stress intensity factor for mode II will be investigated along the crack front. Additionally, a relationship between the stress intensity factor and the distance from a singular point, which is the intersection point of the crack front and the free surface, is derived, and the validity of the relationship will be demonstrated.

2 Method for analysis

Generally, a finite element method is used for analyzing the stress distribution in solid structures. When the finite element method is used, a large number of mesh data and memory are required for accurately analyzing the distributions of singular stresses near the vertex and crack tip in the three-dimensional joints. So, in the present study, a boundary element method is used to calculate the displacement at an arbitrary point in the three-dimensional joint,

$$u_i(q) = \int_{\Omega} [U_{ij}(q, Q)t_j(Q) - T_{ij}u_j(Q)]\mathrm{d}s(Q), \tag{2}$$

where q is an internal point, Q is a point on the boundary, and U_{ij} and T_{ij} are the fundamental solutions for displacement and traction, respectively. In the present analysis, Rongved's solution for two-phase materials

satisfying the boundary condition of the interface is used for the fundamental solution. So, mesh division on the interface in the joint is not needed, and a precise stress analysis can be done. Stresses at the internal point, q, are calculated using the strain obtained from the following equation:

$$u_{i,j}(q, Q) = \int_{\Omega} [U_{ik,j}(q, Q)t_k(Q) - T_{ik,j}(q, Q)u_k(Q)]\mathrm{d}s(Q). \tag{3}$$

Stresses are obtained by substituting the strain into a constitutive equation of the material.

An eigenanalysis is conducted to determine the order of the stress singularity. The eigenequation is derived using the formulation of a finite element method on the basis of the principle of virtual work (see Pageau et al. [17]). In deriving the equation, the displacement field for a spherical coordinate system with an origin at the stress singular point is employed. Then, the following eigenequation with respect to p is derived:

$$\left(p^2\,[\mathbf{A}] + p\,[\mathbf{B}] + [\mathbf{C}]\right)\{\mathbf{u}\} = \mathbf{0} \tag{4}$$

where [**A**], [**B**], [**C**] are matrices, and {**u**} is the displacement vector at nodes. The order of the stress singularity, λ, is obtained from $\lambda = 1 - p$.

3 Model for analysis and analysis condition

In the present study, a three-dimensional joint model composed of silicon and resin is analyzed. Three kinds of joint models with and without a crack at the interface are employed for the analysis. Figure 1 shows the models for the analysis and the size of the joint. The upper material is silicon and the lower is resin. Silicon and resin are used in electronic devices, and these models are prepared for comparing the stress distributions before and after the initiation of crack. Silicon and resin are widely used in semiconductors, where their thicknesses are very thin, the singular stress fields at the vertex of the interface are fairly influenced by the thickness. In the present models, the influence of the thickness of silicon and resin is negligible. In the previous paper, the quantities of energy release due to the occurrence of three differently shaped cracks were investigated (Koguchi et al. [28]). In these joint models, a very small domain is established for making the crack, and a zone method is employed in the boundary element method (BEM) analysis. Figure 2 shows the geometry of the interface crack. The height of the small domain is 0.05 mm in the z-direction, and the cross section in the x–y plane is the same size as the interface crack. Here, a triangular-shaped crack is referred to as Type A, a quarter-circular-shaped crack as Type B, and a concave-shaped crack as Type C. The areas of the three types of cracks are equal to 3.618×10^{-8} mm^2. The lengths of the side lines for the three types of cracks and the coordinates of the center of the circle for Type C are $L_a = 2.69 \times 10^{-4}$ mm, $L_b = 2.15 \times 10^{-4}$ mm, $L_c = 3.05 \times 10^{-4}$ mm, $d = 6.82472 \times 10^{-4}$ mm, and $c = 9.999389648 \times 10^{-4}$ mm, respectively. Figure 3 demonstrates the mesh division around the crack for BEM analysis in Type A. The size of the mesh decreases

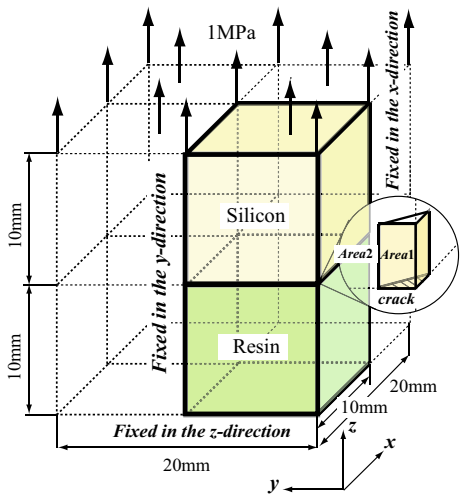

Fig. 1 Analysis model for a three-dimensional joint

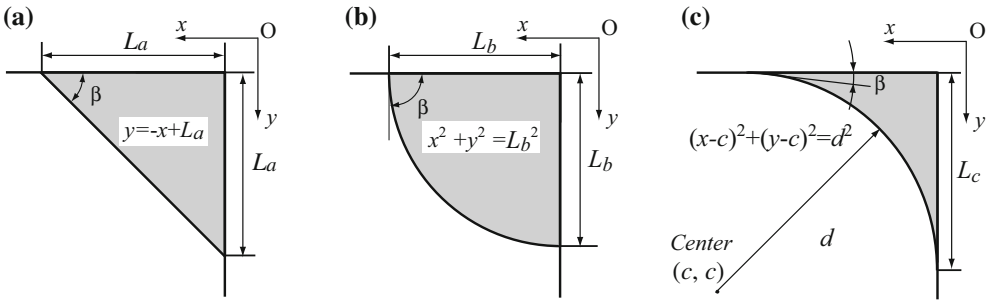

Fig. 2 Crack shapes for analysis

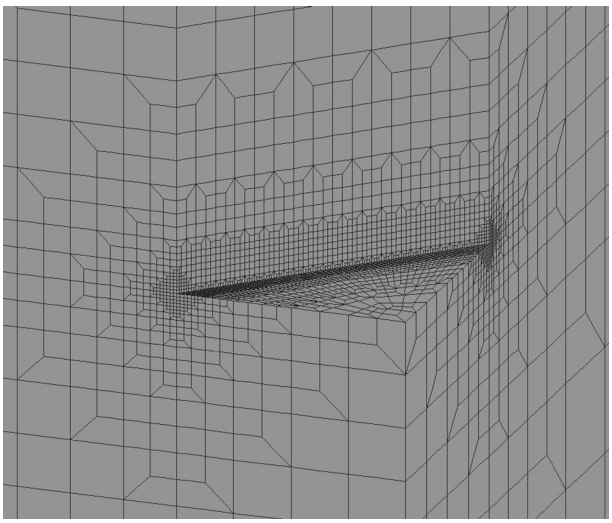

Fig. 3 Mesh division for BEM analysis in Type A

Table 1 Mesh division for BEM analysis

Crack type	Type A	Type B	Type C
Element number	7152	7896	9682
Node number	21,460	22,732	29,149
The minimum element length (mm)	2.63×10^{-6}	2.97×10^{-6}	1.20×10^{-6}

Table 2 Material properties used in the analysis

	Silicon	Resin
Young's modulus (GPa)	166.01	2.74
Poisson's ratio	0.26	0.38

with approaching the crack front, and the minimum size of the element, the total element number, and the total node number for each crack type are shown in Table 1.

A tensile stress of 1 MPa in the z-direction is applied at the upper surface, and the displacement in the z-direction is fixed at the lower surface in the joint model. The upper and lower materials are 10 mm in height and 20 mm in width, respectively. A quarter model of the joint is analyzed considering the symmetry of the boundary condition and the geometry. The material properties used in the analysis are shown in Table 2.

Table 3 Eigenvalues at the interface of silicon–resin

Stress singular point,	$\phi_{op} = 90°$	Stress singular line,	$\phi_{op} = 180°$
$Re(\lambda_{\text{vertex}})$	$Im(\lambda_{\text{vertex}})$	$Re(\lambda_{\text{line}})$	$Im(\lambda_{\text{line}})$
0.395	0.000	0.318	0.000

Table 4 Eigenvalues at a point on the crack tip

$Re(\lambda_1)$	$Re(\lambda_2)$	$Im(\lambda_2)$	$Re(\lambda_3)$	$Im(\lambda_3)$
0.50	0.50	0.0592	0.50	−0.0592

Table 5 Eigenvalues at the intersection point of crack front line and the free surface

Type A,	$\beta = 45°$	Type B,	$\beta = 90°$	Type C,	$\beta = 27.5°$
λ_1	λ_2	λ_1	λ_2	λ_1	λ_2
0.458	0.317	0.673	0.508	0.385	0.144

4 Results of analysis

4.1 Eigenanalysis

The order of the stress singularity at the vertex in the three-dimensional joint for the no-crack model is first calculated. The values at the vertex, λ_{vertex}, and on the stress singularity line, λ_{line}, are shown in Table 3. The value for the vertex is larger than that for the line. Next, the values of the stress singularity at the crack tip are shown in Table 4. Complex stress singularity occurs in the interface crack. Furthermore, the values of the orders of stress singularity at intersection points of the crack front and the side surface are shown in Table 5. Two values yielding the stress singularity exist in every crack type. The values for Type C are the smallest ones in three kinds of crack type.

4.2 Stress analysis

4.2.1 Stress distributions in the model without a crack

First, the stress distribution near the vertex of the interface in the three-dimensional joint for the no-crack model is precisely investigated. Stress components in a Cartesian coordinate system are calculated using Eq. (3), and they are transformed from the Cartesian coordinate system to a spherical coordinate system so that an origin is located at the vertex of the interface. The distributions of stresses, $\sigma_{\theta\theta}$, $\sigma_{r\theta}$, $\sigma_{\phi\theta}$, against the distance from the vertex are shown in Fig. 4a. The superscript of the vertex indicates the stress component at the vertex. It is found that the distributions for different stress components have the same slope of 0.395, which agrees with the result of the eigenanalysis shown in Table 3. Figure 4b shows the distributions of stresses, $\sigma_{\theta\theta}$, $\sigma_{r\theta}$, $\sigma_{\phi\theta}$, versus the angle ϕ, which is the angle from the side surface. The stresses in the singular stress field can be expressed as follows:

$$\sigma_{ij}^{\text{vertex}}(r,\theta,\phi) = K_{1ij} f_{1ij}(\theta,\phi)\, r^{-\lambda_{\text{vertex}}} + K_{2ij} f_{2ij}(\theta,\phi) \tag{5}$$

where θ is the angle from the z-axis, K_{1ij} is the intensity of the singularity, and f_{1ij} and f_{2ij} are the angular functions determined from the eigenanalysis. Here, we focus on the stress distributions in the interface. So, the angular functions, $f_{kij}(\theta,\phi)$, at $\theta = \pi/2$ are referred to as $f_{kij}^{\phi}(\phi)$. When the values of the order of stress singularity for the singular stress line on both side surfaces are identical, the angular functions in the interface can be expressed as follows [25]:

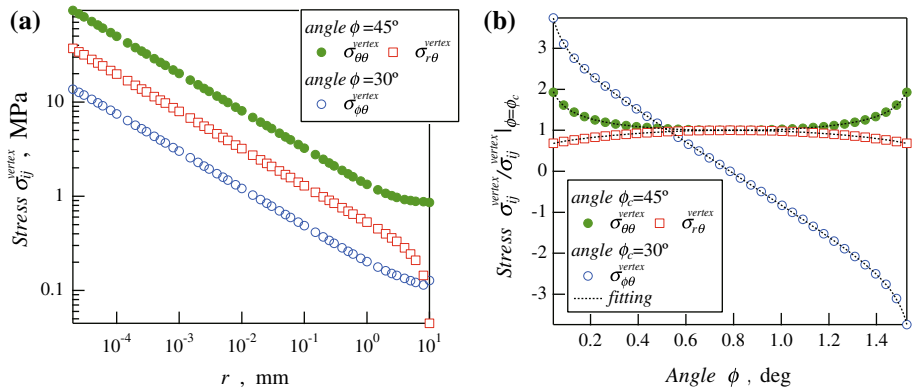

Fig. 4 Distributions of stresses: **a** $\sigma_{ij}^{\text{vertex}}$ versus the distance from the vertex, **b** $\sigma_{ij}^{\text{vertex}}/\sigma_{ij}^{\text{vertex}}|_{\phi=30^\circ,\,45^\circ}$ versus ϕ

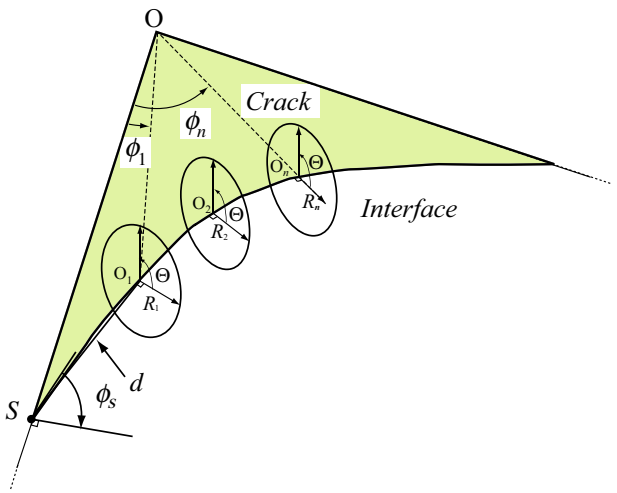

Fig. 5 Local polar coordinate system established along the crack front, and the distance d from the origin to the intersection of the crack front with the side surface

$$f_{1\theta\theta}^{\phi}(\phi) = L_{1\theta\theta}\left\{(\sin\phi)^{-\lambda_{\text{line}}} + (\cos\phi)^{-\lambda_{\text{line}}}\right\} + L_{2\theta\theta}, \tag{6}$$

$$f_{1r\theta}^{\phi}(\phi) = L_{1r\theta}\left\{(\sin\phi)^{-\lambda_{\text{line}}}\cos\phi + (\cos\phi)^{-\lambda_{\text{line}}}\sin\phi\right\} + L_{2r\theta}\left\{(\sin\phi)^{1-\lambda_{\text{line}}} + (\cos\phi)^{1-\lambda_{\text{line}}}\right\} + L_{3r\theta}(\sin\phi + \cos\phi), \tag{7}$$

$$f_{1\phi\theta}^{\phi}(\phi) = L_{1\phi\theta}\left\{(\sin\phi)^{-\lambda_{\text{line}}}\cos\phi - (\cos\phi)^{-\lambda_{\text{line}}}\sin\phi\right\} + L_{2\phi\theta}\left\{(\sin\phi)^{1-\lambda_{\text{line}}} - (\cos\phi)^{1-\lambda_{\text{line}}}\right\} + L_{3\phi\theta}(\sin\phi + \cos\phi) + L_{4\phi\theta}(\cos\phi - \sin\phi). \tag{8}$$

The coefficients in Eqs. (5), (6), (7), and (8) for stress, σ_{ij}, are determined from the plots shown in Fig. 4a, b using the least square method. Then, the determined values are shown in Table 5.

4.2.2 Stress distributions in the model with a small crack

The stress distributions along the interface crack front line are precisely investigated. Here, a polar coordinate system such as shown in Fig. 5 is introduced to examine a relationship between the singular stress fields at the vertex and at the crack tip. S shown in Fig. 5 is an intersection point of the crack front and the side surface, and d is the distance from S to an arbitrary point on the crack front. Figure 5 shows the polar coordinate system, (R, Θ), taken at the crack front. The origin of the polar coordinate is located at d from the point S.

In the present study, the stress component for the mode II is mainly investigated. The distributions of stress, $\sigma_{R\Theta}$, against R for three types of crack shape are shown in Fig. 6. Solid lines indicate the plots of the stress distribution for the no-crack model, and solid circles denote the plots for the crack model. It is found that the stress for crack models is larger than that for the no-crack model in $R < 10^{-4}$ mm, and the slope of lines and

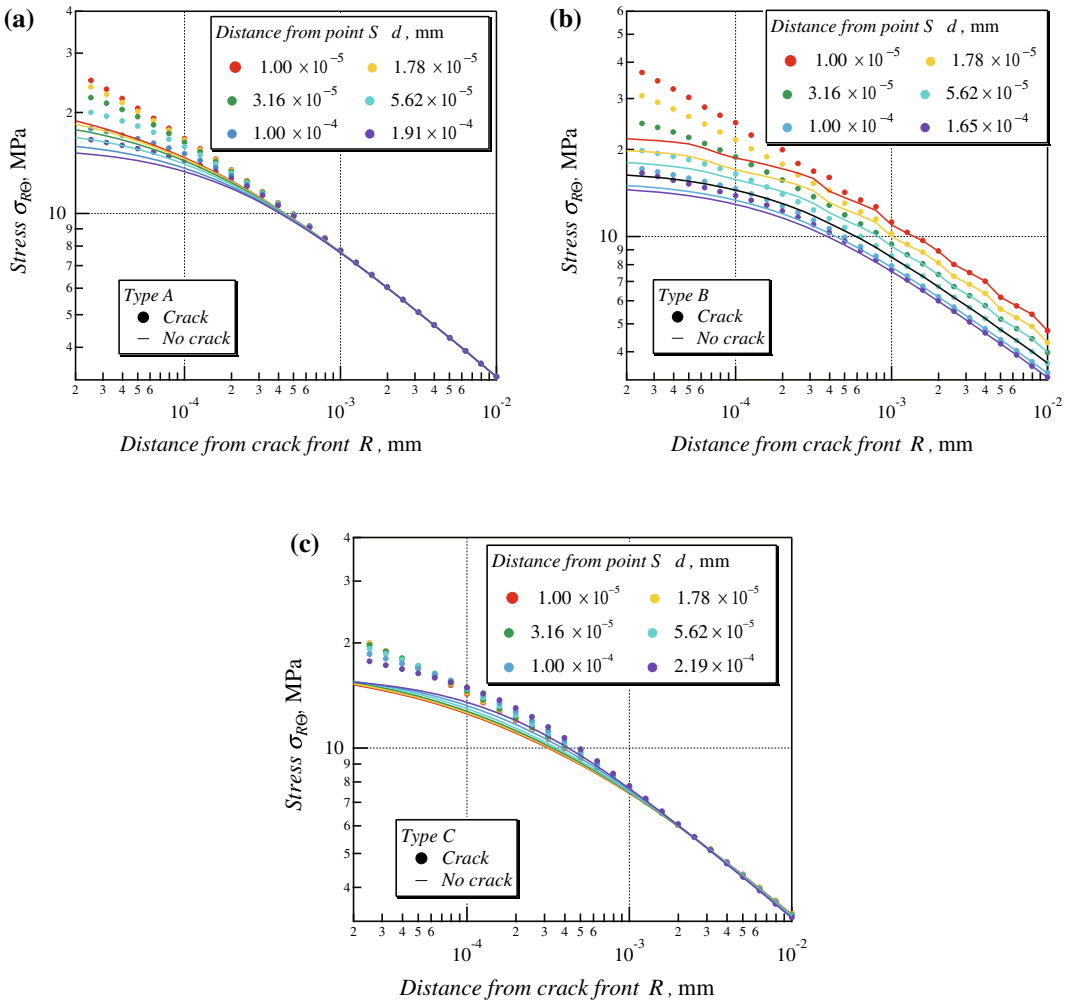

Fig. 6 Comparison of stress distributions for Type A, Type B, and Type C

symbols in the log–log graph agree with each other over $R > 10^{-4}$ mm, where the size of range is about two times the crack length on the side surface. The value of the slope is 0.395, which is the order of singularity at the vertex. Here, the stress $\sigma_{R\Theta}$ is normalized by using the stress in the no-crack model. Figure 7 demonstrates the distribution of the normalized stress against the distance, R, from the crack front. It is found that the stress approaches to a constant value of 1 over $R > 10^{-3}$ mm. When the stress distribution is normalized by the singular stress at the vertex, it can be supposed that a crack is located under a uniform stress. It is found that the stress near the point S is larger than that far from the point.

4.2.3 Stress intensity factor for mode II

In this section, the expression for the stress intensity factor for mode II in a three-dimensional interface crack is derived from the singular stress field at the crack tip. The dimensionless stress $\sigma_{R\Theta}/\sigma_{r\theta}^{\text{vertex}}$ is expressed as $\hat{\sigma}_{R\Theta}(\hat{R}, \Theta)$ and is defined as

$$\hat{\sigma}_{R\Theta}(\hat{R}, \Theta) = \left(\hat{K}_{1R\Theta}(\Theta)\hat{R}^{i\varepsilon} + \hat{\bar{K}}_{1R\Theta}(\Theta)\,\hat{R}^{-i\varepsilon}\right)\hat{R}^{-0.5} + \hat{K}_{2R\Theta}(\Theta) \tag{9}$$

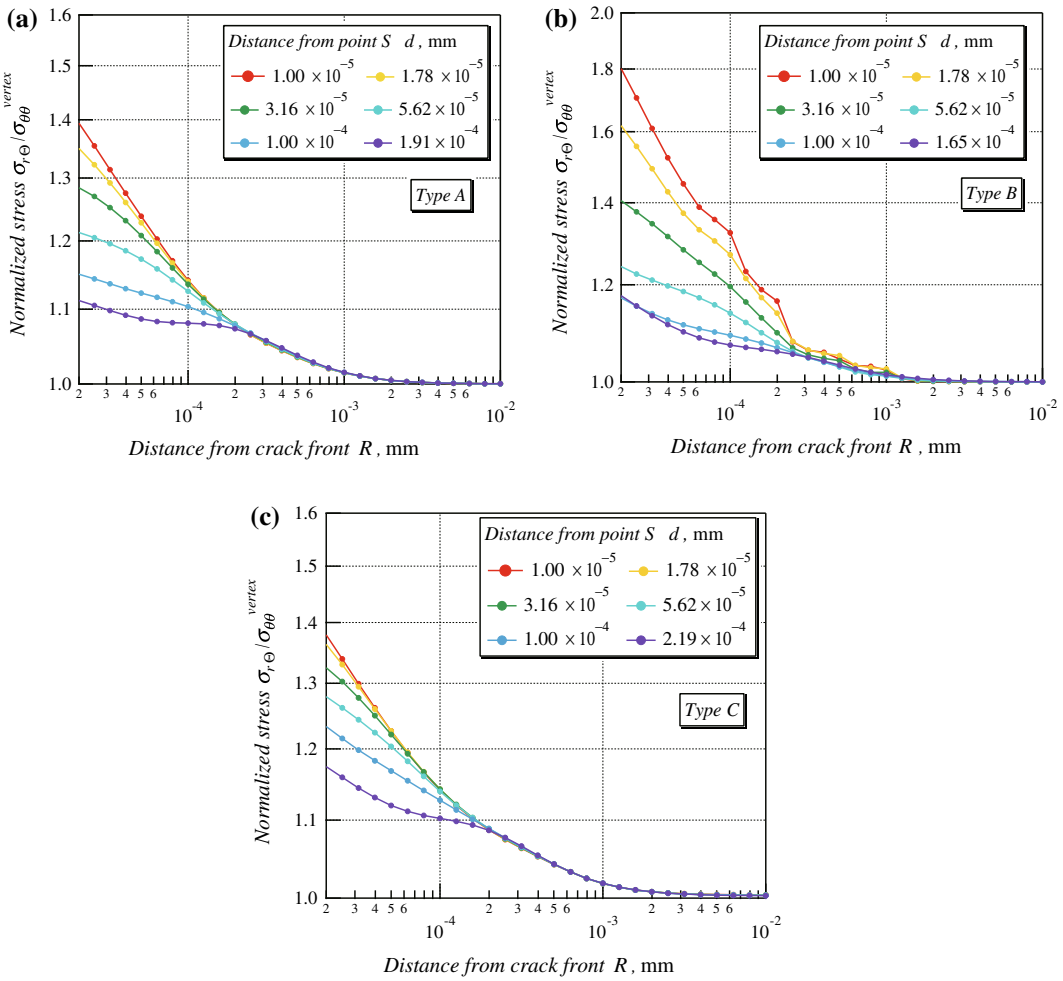

Fig. 7 Comparison of normalized stress distributions for Type A, Type B, and Type C

where $\hat{R} = R/\ell$, ℓ is set as 1×10^{-6} mm (a reference length), and ε is 0.0592. $\hat{K}_{1R\Theta}$ is a dimensionless complex stress intensity factor for mode II and is defined as follows:

$$\begin{aligned} \hat{K}_{1R\Theta} &= \hat{K}_{II}\,\tilde{f}_{1R\Theta} = \hat{K}_{II}\left\{\tilde{f}^{Re}_{1R\Theta}(\Theta) + i\,\tilde{f}^{Im}_{1R\Theta}(\Theta)\right\}, \\ \hat{\bar{K}}_{1R\Theta} &= \hat{K}_{II}\,\bar{\tilde{f}}_{1R\Theta} = \hat{K}_{II}\left\{\tilde{f}^{Re}_{1R\Theta}(\Theta) - i\,\tilde{f}^{Im}_{1R\Theta}(\Theta)\right\} \end{aligned} \tag{10}$$

where $\hat{K}_{II}$ is a real dimensionless stress intensity factor for mode II, and $\tilde{f}_{1R\Theta}$ is the normalized angular function for the complex order of singularity of $-0.5 + i\varepsilon$. $\tilde{f}^{Re}_{1R\Theta}$ and $\tilde{f}^{Im}_{1R\Theta}$ are the real and imaginary parts of the angular functions. The complex angular function, $\tilde{f}_{1R\Theta}(\Theta)$, is derived by normalizing $f_{1R\Theta}$ using the value at the interface of $\left|f^{Re}_{1R\Theta} + i\,f^{Im}_{1R\Theta}\right|$. The values for the angular function at the interface are shown in Table 7,

$$\tilde{f}_{1R\Theta}(\Theta) = \frac{f^{Re}_{1R\Theta} + i\,f^{Im}_{1R\Theta}}{\left|f^{Re}_{1R\Theta} + i\,f^{Im}_{1R\Theta}\right|} = \tilde{f}^{Re}_{1R\Theta} + i\,\tilde{f}^{Im}_{1R\Theta}. \tag{11}$$

Substitution of Eq. (10) into Eq. (9) yields

$$\hat{\sigma}_{R\Theta}\left(\hat{R}, 0\right) = 2\hat{K}_{II}\left\{\tilde{f}^{Re}_{1R\Theta}(0)\cos\left(\varepsilon \ln \hat{R}\right) - \tilde{f}^{Im}_{1R\Theta}\sin\left(\varepsilon \ln \hat{R}\right)\right\}\hat{R}^{-0.5} + \hat{K}_{2R\Theta}(0)\,. \tag{12}$$

Table 6 Values of coefficients in Eqs. (5), (6), (7), and (8)

$K_{1\theta\theta}$, MPa mm$^{\lambda_{\text{vertex}}}$	$K_{2\theta\theta}$, MPa mm	$L_{1\theta\theta}$	$L_{1\theta\theta}$	–	–
1.26	0.0594	0.64	−0.43	–	–
$K_{1r\theta}$, MPa mm$^{\lambda_{\text{vertex}}}$	$K_{2r\theta}$, MPa	$L_{1r\theta}$	$L_{2r\theta}$	$L_{3r\theta}$	–
0.535	−0.00154	−0.0298	0.254	0.458	–
$K_{1\phi\theta}$, MPa mm$^{\lambda_{\text{vertex}}}$	$K_{2\phi\theta}$, MPa mm	$L_{1\phi\theta}$	$L_{2\phi\theta}$	$L_{3\phi\theta}$	$L_{4\phi\theta}$
0.194	0.0263	1.012	0.826	0.0672	1.919

Table 7 Values of the angular function on the interface and crack front

$\left\|f^{Re}_{1R\Theta}(0) + i\, f^{Im}_{1R\Theta}(0)\right\|$	$\tilde{f}^{Re}_{1R\Theta}(0)$	$\tilde{f}^{Im}_{1R\Theta}(0)$
3.28×10^{-4}	0.733	0.680

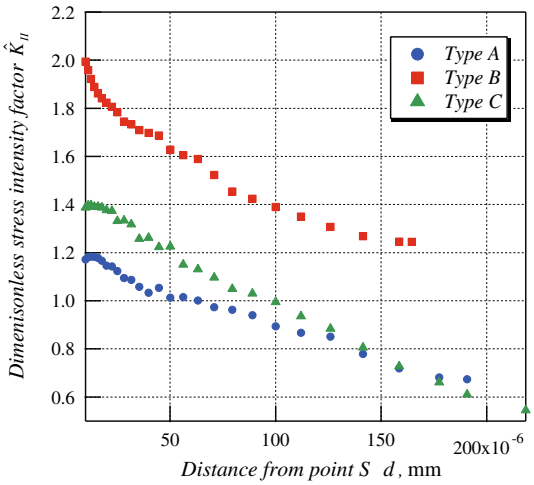

Fig. 8 Variation in $\hat{K}_{II}$ against the distance d from the point S: Type A, Type B, and Type C

Furthermore, the dimensionless stress intensity factor, $\hat{K}_{II}$, is changed into the stress intensity factor with the dimension as

$$K_{II} = 2\sqrt{2\pi}\,\hat{K}_{II}\sigma_{r\theta}^{\text{vertex}}\ell^{0.5} \tag{13}$$

where K_{II} is the real stress intensity factor for mode II. Then, Eq. (12) is rewritten as

$$\sigma_{R\Theta}\left(\hat{R}, 0\right) = \frac{\hat{K}_{II}}{\sqrt{2\pi}}\left\{\tilde{f}^{Re}_{1R\Theta}(0)\cos\left(\varepsilon \ln \hat{R}\right) - \tilde{f}^{Im}_{1R\Theta}\sin\left(\varepsilon \ln \hat{R}\right)\right\}\hat{R}^{-0.5} + K_{2R\Theta}(0) \tag{14}$$

where $K_{2R\Theta}(0)$ is a constant value which is related to the stress far from the crack front.

The dimensionless stress intensity factor, $\hat{K}_{II}$, is obtained approximating the stress distribution shown in Fig. 7 by using Eq. (14). The determined $\hat{K}_{II}$ is plotted against the distance d as shown in Fig. 8. It is found that the values increase as d decreases.

Next, the singular stress fields around the intersection point S are precisely investigated. There are two values for the order yielding the stress singularity as shown in Table 5. Then, the distribution of stress, $\sigma_{r\theta}$, near the point S is expressed as

$$\sigma^s_{r\theta}\left(\hat{r}_s, \frac{\pi}{2}, \phi_s\right) = K^s_{1r\theta}\ell^{-\lambda_1}\hat{f}^{s\ \phi}_{1r\theta}(\phi_s)\,\hat{r}_s^{-\lambda_1} + K^s_{2r\theta}\ell^{-\lambda_2}\hat{f}^{s\ \phi}_{2r\theta}(\phi_s)\,\hat{r}_s^{-\lambda_2} + K^s_{3r\theta}\hat{f}^{s\ \phi}_{3r\theta}(\phi_s) \tag{15}$$

where $\hat{r}_s = r/\ell$, $K^s_{kr\theta}$ and $f^s_{kr\theta}$, $(k = 1, 2)$ are the intensity of singularities and the angular functions for the order of the stress singularity, λ_k, respectively. ϕ_s is an angle taken from the crack front as shown in Fig. 5. Here, the angular functions for each values of the order of singularity are shown in Fig. 9. The angular functions, $f^s_{kr\theta}$, are normalized by the minimum values of $f^s_{k\theta\theta}$. The intensities of singularity, $K^s_{kr\theta}$, are determined from the stress distribution shown in Fig. 10 using a conservative integral developed by the authors [34]. In evaluating

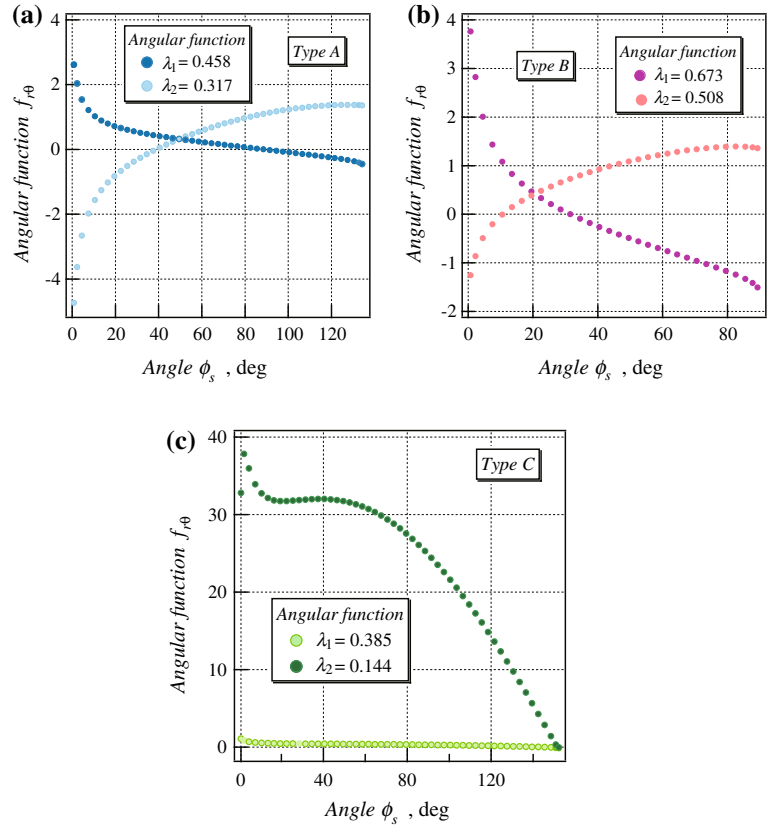

Fig. 9 Distributions of $f_{r\theta}$ against angle ϕ_s for Type A, Type B, and Type C

numerically the conservative integral, the angular functions for the whole domain in the analysis are used. Then, the determined coefficients for each term in Eq. (15) are shown in Table 7.

Next, the singular behavior of the angular functions near the crack front, $\phi_s \approx 0$, is examined. The angular functions, $\tilde{f}^{s\,\phi}_{kr\theta}$, can be expressed versus the angle ϕ_s as follows [25]:

$$\begin{aligned}\tilde{f}^{s\,\phi}_{kr\theta}(\phi_s) = {} & L^{*s}_{1kr\theta}\cos\phi_s(\sin\phi_s)^{-0.5+i\varepsilon} + \bar{L}^{*s}_{1kr\theta}\cos\phi_s(\sin\phi_s)^{-0.5-i\varepsilon} \\ & + L^{*s}_{2kr\theta}(\sin\phi_s)^{0.5+i\varepsilon} + \bar{L}^{*s}_{2kr\theta}(\sin\phi_s)^{0.5-i\varepsilon} + L_{3kr\theta}\sin\phi_s\end{aligned} \tag{16}$$

where $L^{*s}_{jkr\theta}$ and $\bar{L}^{*s}_{jkr\theta}$, $(j = 1, 2)$ are complex intensities of singularity for the angular functions, and are defined as

$$\begin{aligned}L^{*s}_{jkr\theta} &= L^{*}_{kIIj}\left\{\tilde{f}^{Re}_{1R\Theta}(\Theta) + i\,\tilde{f}^{Im}_{1R\Theta}(\Theta)\right\} \\ \bar{L}^{*s}_{jkr\theta} &= L^{*}_{kIIj}\left\{\tilde{f}^{Re}_{1R\Theta}(\Theta) - i\,\tilde{f}^{Im}_{1R\Theta}(\Theta)\right\},\end{aligned} \tag{17}$$

where L^{*}_{kIIj} is a real intensity factor of the angular function, and $\tilde{f}^{Re}_{1R\Theta}$ and $\tilde{f}^{Im}_{1R\Theta}$, $(j = 1,\ 2$ and $k = 1,\ 2)$ are already defined in Eq. (11), as the real and imaginary parts of the angular function at the crack tip, respectively. Substituting Eqs. (16) and (17) into Eq. (15) and expanding the equation yield

$$\begin{aligned}\tilde{f}^{s\,\phi}_{kr\theta}(\phi_s) = {} & 2L^{*}_{kII1}\left\{\tilde{f}^{Re}_{1R\Theta}(0)\cos(\varepsilon\ln(\sin\phi_s)) - \tilde{f}^{Im}_{1R\Theta}(0)\sin(\varepsilon\ln(\sin\phi_s))\right\}(\sin\phi_s)^{-0.5}\cos\phi_s \\ & + 2L^{*}_{kII2}\left\{\tilde{f}^{Re}_{1R\Theta}(0)\cos(\varepsilon\ln(\sin\phi_s)) + \tilde{f}^{Im}_{1R\Theta}(0)\sin(\varepsilon\ln(\sin\phi_s))\right\}(\sin\phi_s)^{0.5} \\ & + L_{3kr\theta}\sin\phi_s.\end{aligned} \tag{18}$$

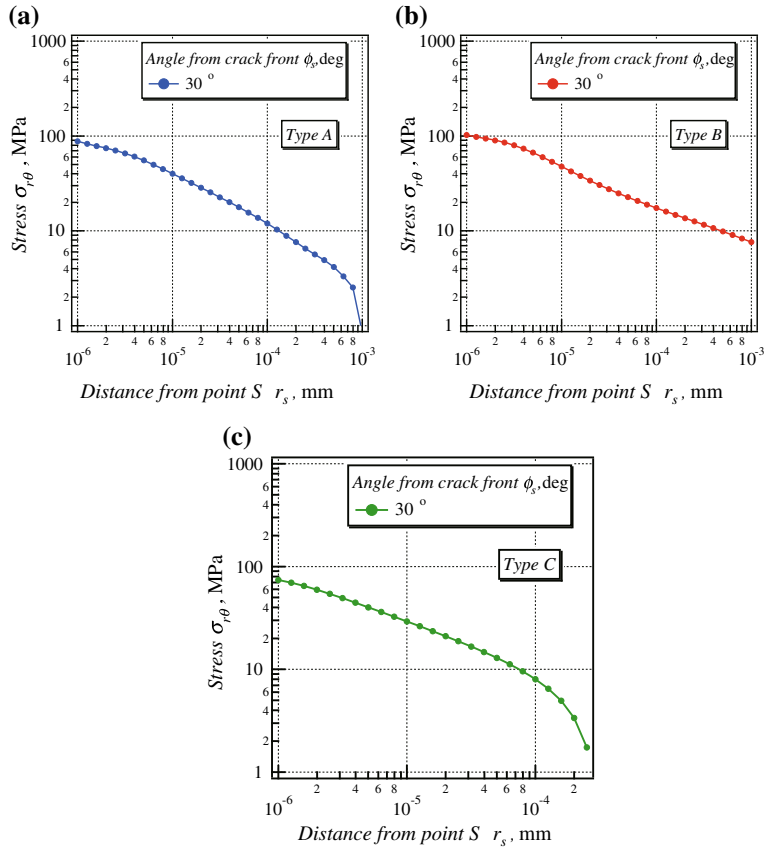

Fig. 10 Distributions of $\sigma_{r\theta}$ against the distance from the point S for Type A, Type B, and Type C

Here, introducing the same relationship of $L^s_{kIIj} = 2\sqrt{2\pi}L^*_{kIIj}$ as the crack front into the angular function yields the following equation:

$$\begin{aligned}\tilde{f}^{s\,\phi}_{kr\theta}(\phi_s) = {} & \frac{L^s_{kII1}}{\sqrt{2\pi}}\left\{\tilde{f}^{Re}_{1R\Theta}(0)\cos(\varepsilon\ln(\sin\phi_s)) - \tilde{f}^{Im}_{1R\Theta}(0)\sin(\varepsilon\ln(\sin\phi_s))\right\}(\sin\phi_s)^{-0.5}\cos\phi_s \\ & + \frac{L^s_{kII2}}{\sqrt{2\pi}}\left\{\tilde{f}^{Re}_{1R\Theta}(0)\cos(\varepsilon\ln(\sin\phi_s)) + \tilde{f}^{Im}_{1R\Theta}(0)\sin(\varepsilon\ln(\sin\phi_s))\right\}(\sin\phi_s)^{0.5} \\ & + L_{3kr\theta}\sin\phi_s. \end{aligned} \tag{19}$$

Now, the coefficients, L^s_{kIIj}, are determined from the approximation of the angular functions shown in Fig. 9 at the interface by Eq. (19). The obtained coefficients, L^s_{kII1}, are shown in Table 8

Next, Eq. (19) is substituted into Eq. (15); then, the following equation is derived:

$$\begin{aligned}&\sigma^s_{r\theta}\left(\hat{r}_s, \frac{\pi}{2}, \phi_s\right) \\ &= K^s_{1r\theta}\ell^{-\lambda_1}\left[\begin{array}{l}\frac{L^s_{1II1}}{\sqrt{2\pi}}\left\{\tilde{f}^{Re}_{1R\Theta}(0)\cos(\varepsilon\ln(\sin\phi_s)) - \tilde{f}^{Im}_{1R\Theta}(0)\sin(\varepsilon\ln(\sin\phi_s))\right\}(\sin\phi_s)^{-0.5}\cos\phi_s \\ +\frac{L^s_{1II2}}{\sqrt{2\pi}}\left\{\tilde{f}^{Re}_{1R\Theta}(0)\cos(\varepsilon\ln(\sin\phi_s)) + \tilde{f}^{Im}_{1R\Theta}(0)\sin(\varepsilon\ln(\sin\phi_s))\right\}(\sin\phi_s)^{0.5} \\ +L^s_{1II3}\sin\phi_s\end{array}\right]\hat{r}_s^{-\lambda_1} \\ &+ K^s_{2r\theta}\ell^{-\lambda_2}\left[\begin{array}{l}\frac{L^s_{2II1}}{\sqrt{2\pi}}\left\{\tilde{f}^{Re}_{1R\Theta}(0)\cos(\varepsilon\ln(\sin\phi_s)) - \tilde{f}^{Im}_{1R\Theta}(0)\sin(\varepsilon\ln(\sin\phi_s))\right\}(\sin\phi_s)^{-0.5}\cos\phi_s \\ +\frac{L^s_{2II2}}{\sqrt{2\pi}}\left\{\tilde{f}^{Re}_{1R\Theta}(0)\cos(\varepsilon\ln(\sin\phi_s)) + \tilde{f}^{Im}_{1R\Theta}(0)\sin(\varepsilon\ln(\sin\phi_s))\right\}(\sin\phi_s)^{0.5} \\ +L^s_{2II3}\sin\phi_s\end{array}\right]\hat{r}_s^{-\lambda_2} \\ &+ K^s_{3r\theta}\tilde{f}^{s\,\phi}_{3r\theta}. \end{aligned} \tag{20}$$

Table 8 Values of coefficients in Eq. (15)

	Type A		Type B		Type C	
λ_k	0.458	0.317	0.673	0.508	0.385	0.144
$K^s_{kr\theta}$, MPa mm$^{\lambda_k}$	0.417	0.632	0.0219	0.205	0.920	0.771

Table 9 Values of coefficients, $L^s_{kI\!I1}$

	Type A		Type B		Type C	
λ_k	0.458	0.317	0.673	0.508	0.385	0.144
$L^s_{kI\!Ij}$	−2.09	1.13	−0.441	1.96	0.852	−6.60

Now, considering the stress distribution near the crack front and simplifying as $\sin\phi_s \approx \phi_s$, $\cos\phi_s \simeq 1$, $\hat{r}_s \simeq \hat{d}_s$ and $\hat{R} = \hat{d}\tan\phi_s \simeq \hat{d}\sin\phi_s \simeq \hat{d}\phi_s$ yield

$$
\begin{aligned}
&\sigma^s_{r\theta}\left(\hat{r}_s, \frac{\pi}{2}, \phi_s\right) \\
&= \frac{K^s_{1r\theta}\ell^{0.5-\lambda_1}L^s_{1I\!I1}}{\sqrt{2\pi}}\left\{\begin{array}{l}\left[\tilde{f}^{Re}_{1R\Theta}(0)\cos\left(\varepsilon\ln\hat{d}\right)+\tilde{f}^{Im}_{1R\Theta}(0)\sin\left(\varepsilon\ln\hat{d}\right)\right]\cos(\varepsilon\ln\hat{R}) \\ +\left[\tilde{f}^{Re}_{1R\Theta}(0)\sin\left(\varepsilon\ln\hat{d}\right)-\tilde{f}^{Im}_{1R\Theta}(0)\cos\left(\varepsilon\ln\hat{d}\right)\right]\sin(\varepsilon\ln\hat{R})\end{array}\right\}R^{-0.5}\hat{d}^{0.5-\lambda_1} \\
&\quad+\frac{K^s_{1r\theta}\ell^{-0.5-\lambda_1}L^s_{1I\!I2}}{\sqrt{2\pi}}\left\{\begin{array}{l}\left[\tilde{f}^{Re}_{1R\Theta}(0)\cos\left(\varepsilon\ln\hat{d}\right)-\tilde{f}^{Im}_{1R\Theta}(0)\sin\left(\varepsilon\ln\hat{d}\right)\right]\cos(\varepsilon\ln\hat{R}) \\ +\left[\tilde{f}^{Re}_{1R\Theta}(0)\sin\left(\varepsilon\ln\hat{d}\right)+\tilde{f}^{Im}_{1R\Theta}(0)\cos\left(\varepsilon\ln\hat{d}\right)\right]\sin(\varepsilon\ln\hat{R})\end{array}\right\}R^{0.5}\hat{d}^{-0.5-\lambda_1} \\
&\quad+K^s_{1r\theta}\ell^{-1-\lambda_1}L^s_{1I\!I3}R\hat{d}^{-1-\lambda_1} \\
&\quad+\frac{K^s_{2r\theta}\ell^{0.5-\lambda_2}L^s_{2I\!I1}}{\sqrt{2\pi}}\left\{\begin{array}{l}\left[\tilde{f}^{Re}_{1R\Theta}(0)\cos\left(\varepsilon\ln\hat{d}\right)+\tilde{f}^{Im}_{1R\Theta}(0)\sin\left(\varepsilon\ln\hat{d}\right)\right]\cos(\varepsilon\ln\hat{R}) \\ +\left[\tilde{f}^{Re}_{1R\Theta}(0)\sin\left(\varepsilon\ln\hat{d}\right)-\tilde{f}^{Im}_{1R\Theta}(0)\cos\left(\varepsilon\ln\hat{d}\right)\right]\sin(\varepsilon\ln\hat{R})\end{array}\right\}R^{-0.5}\hat{d}^{0.5-\lambda_2} \\
&\quad+\frac{K^s_{2r\theta}\ell^{-0.5-\lambda_2}L^s_{2I\!I2}}{\sqrt{2\pi}}\left\{\begin{array}{l}\left[\tilde{f}^{Re}_{1R\Theta}(0)\cos\left(\varepsilon\ln\hat{d}\right)-\tilde{f}^{Im}_{1R\Theta}(0)\sin\left(\varepsilon\ln\hat{d}\right)\right]\cos(\varepsilon\ln\hat{R}) \\ +\left[\tilde{f}^{Re}_{1R\Theta}(0)\sin\left(\varepsilon\ln\hat{d}\right)+\tilde{f}^{Im}_{1R\Theta}(0)\cos\left(\varepsilon\ln\hat{d}\right)\right]\sin(\varepsilon\ln\hat{R})\end{array}\right\}R^{0.5}\hat{d}^{-0.5-\lambda_2} \\
&\quad+K^s_{2r\theta}\ell^{-1-\lambda_2}L^s_{2I\!I3}R\hat{d}^{-1-\lambda_2} \\
&\quad+K^s_{3r\theta}\tilde{f}^{s\,\phi}_{3r\theta}.
\end{aligned}
\tag{21}
$$

Comparing the coefficients of $\cos(\varepsilon\ln\hat{R})$ and $\sin(\varepsilon\ln\hat{R})$ in Eqs. (12) and (21) yields the following equations:

$$
\begin{aligned}
K_{I\!I}\tilde{f}^{Re}_{1R\Theta}(0) &= \left(K^s_{1r\theta}L^s_{1I\!I1}d^{0.5-\lambda_1}+K^s_{2r\theta}L^s_{2I\!I1}d^{0.5-\lambda_2}\right)\left\{\tilde{f}^{Re}_{1R\Theta}(0)\cos\left(\varepsilon\ln\hat{d}\right)+\tilde{f}^{Im}_{1R\Theta}(0)\sin\left(\varepsilon\ln\hat{d}\right)\right\} \\
K_{I\!I}\tilde{f}^{Im}_{1R\Theta}(0) &= \left(K^s_{1r\theta}L^s_{1I\!I1}d^{0.5-\lambda_1}+K^s_{2r\theta}L^s_{2I\!I1}d^{0.5-\lambda_2}\right)\left\{\tilde{f}^{Re}_{1R\Theta}(0)\sin\left(\varepsilon\ln\hat{d}\right)-\tilde{f}^{Im}_{1R\Theta}(0)\cos\left(\varepsilon\ln\hat{d}\right)\right\}.
\end{aligned}
\tag{22}
$$

Summing the square of Eq. (22) yields

$$
\begin{aligned}
&K^2_{I\!I}\left\{\left(\tilde{f}^{Re}_{1R\Theta}(0)\right)^2+\left(\tilde{f}^{Im}_{1R\Theta}(0)\right)^2\right\} \\
&\quad=\left(K^s_{1r\theta}L^s_{1I\!I1}d^{0.5-\lambda_1}+K^s_{2r\theta}L^s_{2I\!I1}d^{0.5-\lambda_2}\right)^2\left[\begin{array}{l}\left\{\tilde{f}^{Re}_{1R\Theta}(0)\cos\left(\varepsilon\ln\hat{d}\right)+\tilde{f}^{Im}_{1R\Theta}(0)\sin\left(\varepsilon\ln\hat{d}\right)\right\}^2 \\ +\left\{\tilde{f}^{Re}_{1R\Theta}(0)\sin\left(\varepsilon\ln\hat{d}\right)-\tilde{f}^{Im}_{1R\Theta}(0)\cos\left(\varepsilon\ln\hat{d}\right)\right\}^2\end{array}\right]
\end{aligned}
\tag{23}
$$

where $\left(\tilde{f}^{Re}_{1R\Theta}(0)\right)^2+\left(\tilde{f}^{Im}_{1R\Theta}(0)\right)^2=1$. Then, Eq. (23) is simplified as

$$
K_{I\!I} = K^s_{1r\theta}L^s_{1I\!I1}d^{0.5-\lambda_1}+K^s_{2r\theta}L^s_{2I\!I1}d^{0.5-\lambda_2}. \tag{24}
$$

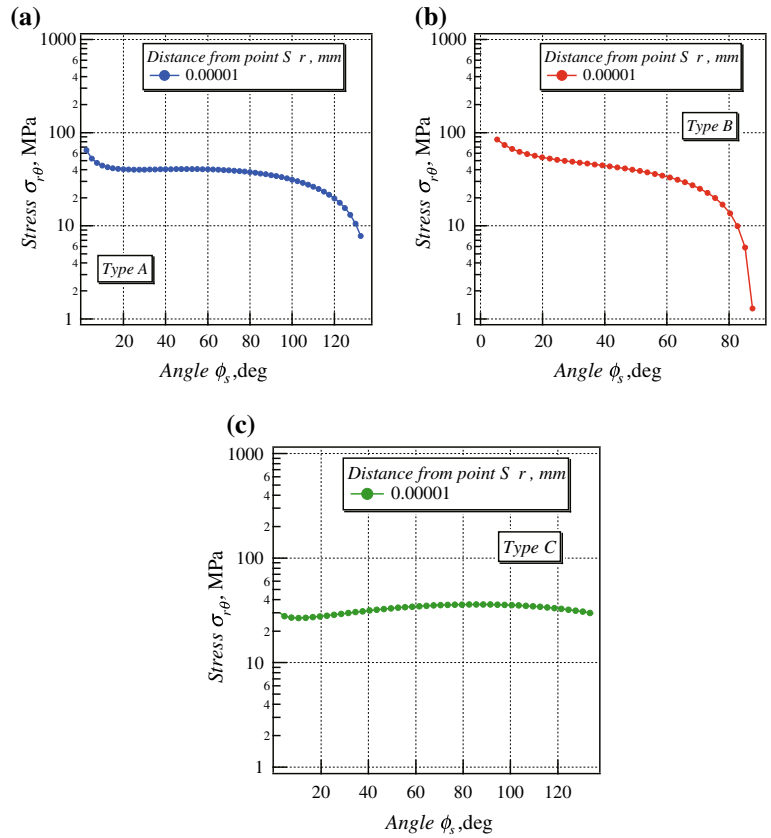

Fig. 11 Distributions of $\sigma_{r\theta}$ versus angle ϕ_s for Type A, Type B, and Type C

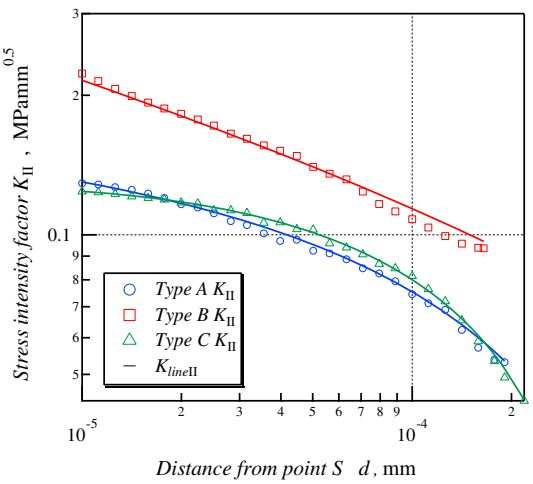

Fig. 12 Distributions of K_{II} against the distance d for Type A, Type B, and Type C

This equation means that the stress intensity factor for the mode II can be expressed as a function of the distance from the point S, and the coefficients for each term were already determined from the approximation of stress distribution and the angular functions for the singular stress distribution at the intersection point S. The right side in Eq. (24) is referred as K_{lineII}, and the value of K_{II} obtained from data shown in Fig. 8 using Eq. (13) and K_{lineII} is replotted in both log graphs. The plotted lines indicate the curves of K_{lineII}. You can see that K_{II} which is determined from the stress distribution in the normal direction to the crack front fairly agrees with

the curves of K_{lineII}. It can be said that the stress intensity factors near the free surface vary with the distance from the singular stress point at the intersection of the crack front and the free surface.

The value of K_{II} is less than that of K_I, and the governing factor of crack growth in the joint is mainly the mode I [29]. However, it is supposed that the shear stress singularity is related to the crack growth near the intersection point due to the increase in the value of K_{II} at the point. Then, the crack shape of Type B tends to grow like that of Type A and Type C. In these joints, the singular stress fields with a distinct character from those at the crack front, $-0.5 \pm i\varepsilon$, exist at the intersection point on the free surface. In the previous numerical analysis of the stress intensity factor near the free surface [15,30], the value was determined at a point on the crack front. Namely, almost all works for three-dimensional surface cracks were to investigate the distribution of stress intensity factors from an inner point on the crack tip to the intersection point of the free surface and the crack front. On the contrary, the distribution of the stress intensity factor is evaluated from the intersection point to the point on the crack tip in this paper. This approach is based on the analysis of singular stress fields in the three-dimensional joints and is applicable to reveal a law of surface crack growth. The results in the paper are limited to interface cracks; however, this approach will be easily extended to any surface cracks.

The deduced results are utilized for evaluating the interface strength not considering the influence of thickness of silicon and resin. In real electronic devices, they are very thin; then, the intensity of singularity at the vertex of the interface reduces [24]. So, the present results yield a reference value for evaluating the interface strength.

5 Conclusions

In the present paper, the stress distribution for three kinds of a very small crack occurring at the vertex of the interface in the three-dimensional joint was analyzed under a tensile load using the boundary element method, and the stress intensity factors for mode II along the crack front line were investigated. The stress intensity factor of mode II varies following a function of the distance from the intersection of the crack front and the free surface to a point on the crack front. The function is expressed by the sum of the exponential function with a power index of the difference in the stress singularities at the cross point at the free surface and at the crack tip (0.5). This expression is very useful for evaluating the growth of a surface crack along an interface.

Acknowledgments We would like to express a sincere gratitude for the support of Grant-in-Aid for Scientific Research (B) 21360051 in Japan.

References

1. Bogy, D.B.: Two edge-bonded elastic wedges of different materials and wedge angles under surface tractions. J. Appl. Mech. **38**, 377–386 (1971)
2. Bogy, D.B., Wang, K.C.: Stress singularities at interface corners in bonded dissimilar isotropic elastic materials. Int. J. Solids Struct. **7**, 993–1005 (1971)
3. Dundurs, J.: Edge-bonded dissimilar orthogonal elastic wedges under normal and shear loading. J. Appl. Mech. **36**, 650–652 (1969)
4. Dempsey, J.P., Sinclair, G.B.: On the stress singularities in the plane elasticity of the composite wedge. J. Elast. **9**, 373–391 (1979)
5. Dempsey, J.P., Sinclair, G.B.: On the singular behavior at the vertex of a bi-material wedge. J. Elast. **11**, 317–327 (1981)
6. Munz, D., Yang, Y.Y.: Stress near the edge of bonded dissimilar materials described by two stress intensity factors. Int. J. Fract. **60**, 169–177 (1993)
7. Banks-Sills, L., Sherer, A.: A conservative integral for determining stress intensity factors of a bimaterial notch. Int. J. Fract. **115**, 1–26 (2002)
8. Luangarpa, C., Koguchi, H.: Intensity of singularity in three-material joints under shear loading: two-real singularities and power-logarithmic singularities. Euro. J. Mech. A Solids **40**, 60–68 (2013)
9. Glushkov, E.V., Glushkova, N.V., Munz, D., Yang, Y.Y.: Analytical solution for bonded wedges under thermal stresses. Int. J. Fract. **106**, 321–339 (2000)
10. Qian, Z.Q., Akisanya, A.R., Thompson, D.S.: Stress behavior at the interface junction of an elastic inclusion. J. Appl. Mech. **69**, 844–852 (2002)
11. Goglio, L., Rossetto, M.: Stress intensity factor in bonded joints: influence of the geometry. Int. J. Adhes. **30**, 313–321 (2010)
12. Qian, Z.Q., Akisanya, A.R.: Stress distribution at the interface corner of a Tri-material structure. J. Eng. Mech. **127**, 747–753 (2001)
13. Koguchi, H., Luangarpa, C.: Two-dimensional joint analysis under shear loading using enriched finite element. J. Solid Mech. Mater. Eng. **2**, 319–332 (2008)

14. Kuo, T-L., Hwu, C.: Multi-order stress intensity factors along three-dimensional interface corners. J. Appl. Mech. **77**, 031020-1–031020-12 (2010)
15. Hwu, C., Huang, H.Y.: Investigation of the stress intensity factors for interface corners. Eng. Fract. Mech. **93**, 204–224 (2012)
16. Pageau, S.S., Joseph, P.F., Biggers, S.B.: The order of stress singularities for bonded and disbanded three-material junction. Int. J. Solids Struct. **31**, 2979–2997 (1994)
17. Pageau, S.S., Bigger, S.B. Jr.: Finite element evaluation of free-edge singular stress fields in anisotropic materials. Int. J. Numer. Methods Eng. **38**, 2225–2239 (1995)
18. Koguchi, H., Muramoto, T.: The order of stress singularity near the vertex in three-dimensional joints. Int. J. Solids Struct. **37**, 4737–4762 (2000)
19. Mittelstedt, C., Becker, W.: Efficient computation of order and mode of three-dimensional stress singularities in linear elasticity by the boundary finite element method. Int. J. Solids Struct. **43**, 2868–2903 (2006)
20. Koguchi, H., Meo, N.: An evaluation of interface strength at a vertex in a three-dimensional joint considering residual thermal stresses using three dimensional boundary element method. Trans. Jpn. Soc. Mech. Eng. **72-723**, 1598–1606 (2006)
21. Monchai, P., Koguchi, H.: Boundary element analysis of the stress field at the singularity lines in three-dimensional bonded joints under thermal loading. J. Mech. Mater. Struct. **2-1**, 149–166 (2007)
22. Koguchi, H., Taniguchi, T.: Characteristics of stress singularity field of residual thermal stresses at vertex in three-dimensional bonded joints. Trans. Jpn. Soc. Mech. Eng. Ser. A **74-724**, 864–872 (2008)
23. Koguchi, H., Konno, N.: Intensity of residual thermal stresses at the vertex in three-dimensional joints with three layers. Trans. Jpn. Soc. Mech. Eng. Ser. A **75**, 1148–1155 (2009)
24. Koguchi, H., Nakajima, M.: Influence of interlayer thickness on the intensity of singular field in 3D three-layered joints under an external load. Trans. Jpn. Soc. Mech. Eng. Ser. A **76**, 1110–1118 (2010)
25. Koguchi, H., da Costa, J.A.: Analysis of the stress singularity field at a vertex in 3D-bonded structures having a slanted side surface. Int. J. Solids Struct. **47**, 3131–3140 (2010)
26. Chiu, Sou-Hsiung J., Chaudhuri, A.: A three-dimensional eigenfunction expansion approach for singular stress field near an adhesively-bonded scarf joint interface in a rigidly-encased plate. Eng. Fract. Mech. **78**, 2220–2234 (2011)
27. Koguchi, H., Hoshi, K.: Evaluation of joining strength of silicon–resin interface at a vertex in a three-dimensional joint structure. J. Electron. Packag. **134**, 020902-1–020902-7 (2012)
28. Koguchi, H., Kimura, N.: Stress analysis near a small crack within singular stress field in a three-dimensional bonded joint under a tensile load. Trans. Jpn. Soc. Mech. Eng. **80**, 1148–1155 (2014)
29. Koguchi, H., Yokoyama, K., Luangarpa, C.: Variation of stress intensity factor along a small interface crack front in singular stress fields. Int. J. Solids Struct. **71**, 156–168 (2015)
30. Nagai, M., Ikeda, T., Miyazaki, N.: Stress intensity factor analysis of a three-dimensional interface crack between dissimilar anisotropic materials. Eng. Fract. Mech. **74**, 2481–2497 (2007)
31. Zhu, B., Shi, Y., Qin, T., Sukop, M., Yu, S., Li, Y.: Mixed-mode stress intensity factors of 3D interface crack in fully coupled electromagnetothermoelastic multiphase composites. Int. J. Solids Struct. **46**, 2669–2679 (2009)
32. Chiu, T.-C., Lin, H.-C.: Analysis of stress intensity factors for three-dimensional interface crack problems in electronic packages using the virtual crack closure technique. Int. J. Fract. **156**, 75–96 (2009)
33. Veluri, B., Jensen, H.M.: Steady-state propagation of interface corner crack. Int. J. Solids Struct. **50**, 1613–1620 (2013)
34. Luangarpa, C., Koguchi, H.: Analysis of a three-dimensional dissimilar material joint with one real singularity using a conservative integral. Int. J. Solids Struct. **51**, 2908–2919 (2014)